

# Properties of moiré magnifiers

## Hala Kamal

Ciudad Universitaria  
Universidad Complutense de Madrid  
Facultad de Físicas  
Departamento de Optica  
28040 Madrid, Spain  
E-mail: j.alda@fis.ucm.es

## Reinhard Völkel

Université de Neuchâtel  
Institute of Microtechnology  
Rue A.-L. Breguet 2  
CH-2000 Neuchâtel  
Switzerland

## Javier Alda

Ciudad Universitaria  
Universidad Complutense de Madrid  
Facultad de Físicas  
Departamento de Optica  
28040 Madrid, Spain

**Abstract.** Moiré magnification can be observed visually if an array of identical objects is viewed through an array of identical microlenses with a different period. Theoretical analysis and experimental results of the moiré image obtained by a moiré magnifier are presented. Conditions for erect and inverted moiré magnifications are derived and interpreted. Virtual erect images are observed only when the period of the lens array is larger than that of the object array, while inverted images are obtainable in both cases. For equal periods, a uniform field of view results. The relation between the relative size of the periods and the distance between the object and the lens arrays are derived. Expressions for image magnification, orientation and size are deduced. The condition to obtain a demagnified moiré pattern is deduced. Rotation of the lens array with respect to the object array results in rotation of the erect and inverted moiré patterns in similar and opposite directions, respectively. © 1998 Society of Photo-Optical Instrumentation Engineers. [S0091-3286(98)00611-4]

Subject terms: moiré effect; microlens arrays.

Paper 01117 received Nov. 3, 1997; revised manuscript received June 3, 1998; accepted for publication June 22, 1998.

## 1 Introduction

The term moiré is a French word meaning “watered moiré,” a glossy cloth with wavy alternating patterns that change forms as the wearer moves. It can also refer to the “watery and wavy” appearance when layers of silk are pressed together by special techniques.<sup>1</sup> Physically, it is an optical phenomenon resulting from the superposition of two or more periodic grid structures. The resulting moiré pattern is influenced by changing any of the three geometrical parameters characterizing the individual grid structures, namely, period, orientation and shape.<sup>1-3</sup>

Although there is a long history in the investigation of superposition moiré effects, only few publications exist that describe the moiré effects appearing if a periodic array of identical objects is observed through a periodic microlens array.<sup>4,5</sup> However, this moiré magnification effect, as we call the phenomenon, is well known from integral images and integral photography.<sup>6,7</sup> The frequent appearance of similar phenomenon in the usage of microlens arrays in conjunction with arrays of light sources, photodetectors, liquid crystals displays, CCD chips, etc. motivates further investigation of this phenomena.<sup>8</sup>

The term “moiré magnifier” is suggested by the conjunction of a periodic object seen through a periodic array of optical elements or systems. The image is formed as the composition, side by side, of the individual images generated by the optical array. The image formation is equal to superposition compound eyes such as nocturnal insects and deep-water crustaceans have.<sup>9</sup> The foundations of optical array design also demonstrate the existence of cooperative effects.<sup>10</sup> In optical array design, the composed image is called as the synthetic image. Using this last approach, the moiré magnifier system should be called a “synthetic magnifier.” However, we prefer to keep the term moiré magnifier

because of the good acceptance of this term by the optics community after the presentation of the device by Hutley et al.<sup>4</sup>

The paper from Hutley et al.<sup>4</sup> dealt with an object array combined with a lens array whose periods are nearly the same size. Experimental results for the magnification and orientation of moiré images and their fundamental dependence on the orientation of the lens array have been given. In our investigation, we explain the formation of erect and inverted moiré images for a moiré magnifier consisting of microlens and object arrays with different periods. We derive the relation between the relative period differences of the arrays and the object array position in  $x$ ,  $y$ ,  $z$  and  $\theta$ . We describe the rotation properties of moiré magnifiers.

## 2 Fundamental Properties of a Moiré Magnifier

The basic configuration of a moiré magnifier is shown in Figure 1. An array of identical objects [Figure 1(b)] is imaged by an array of identical lenses [Figure 1(c)]. For certain combinations of object and lens arrays, one or more magnified moiré images of the object motif are observed [Figure 1(d)]. We now derive the general properties of moiré magnification. For simplicity, we restrict our investigation to symmetrical square arrays. However, a variety of different array types (hexagonal, rhombic, etc.) might be used for moiré magnification in a similar way.

The object array shown in Figure 1 consists of  $O \times O$  identical objects or motifs at a period  $\Lambda_O$ . The lens array consists of  $L \times L$  identical lenses of  $\Phi_L$  aperture at a period  $\Lambda_L$ . The focal length of the lenses is  $f > 0$  (positive lens). Each lens images a part of the object array. The actual type or shape of the lenses (circular or square aperture, refractive or diffractive lens, etc.) is not relevant for our investi-

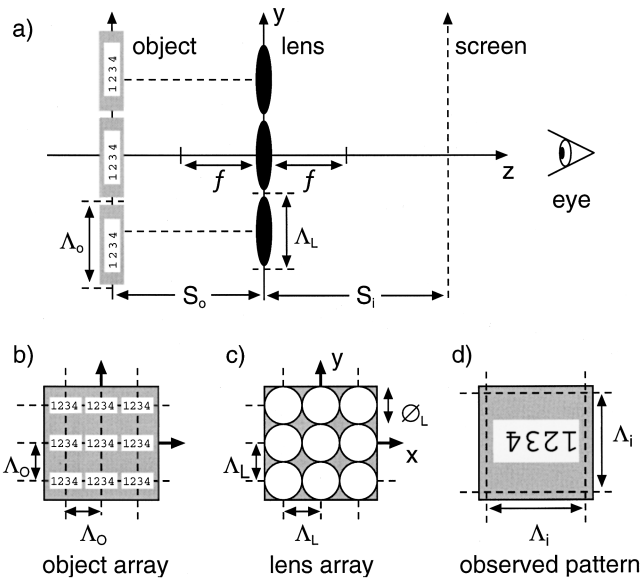


**Fig. 1** Basic configuration of a moiré magnifier. A symmetric square array of identical objects is imaged by a symmetric square array of identical lenses. The object pitch is  $\Lambda_o$ , the lens aperture is  $\Phi_L$ , and the lens pitch is  $\Lambda_L$ . The distance between object plane and lens array is  $s_o$ . The moiré pattern is either observed on a screen located in the image plane at  $s_i$ , or visually in any plane behind the lens array.

gation. We assume that the lens size is equal to the lens period  $\Phi_L = \Lambda_L$ , and ignore all rays not hitting the lenses. The plane of the object array is parallel to the plane of the lens array. The distance between the object plane and the lens array is  $s_o$ . The period of the object array is different from the lens period  $\Lambda_o \neq \Lambda_L$ . The moiré image is either observed on a screen located at  $s_i$  or visually in any plane behind the lens array.

The first fundamental condition for moiré magnification requires that adjacent lenses image adjacent portions  $p_o$  from the object motif. Figure 2 shows examples for an object motif consisting of “1234.” If one lens images the 1, the next neighboring lenses (left and right) should image the 4 or 2 to generate a complete moiré image of the object motif. However, the 4 or 2 portion might be next to 1 or at a certain distance.

An object portions  $p_o$  corresponds to an image of the size  $p_i = p_o m$ , where  $m$  is the magnification factor. Images of different object portions combine to form  $I \times I$  magnified moiré images.

The size of an object portion  $p_o$  imaged by one lens is given by

$$p_o = \Lambda_o \frac{I}{L}, \tag{1}$$

where  $(L/I)^2$  is the number of lenses required to generate a complete moiré image of the object motif (for square arrays). To ensure a coincident superposition of all partial images, the image size  $p_i$  should be equal to the lens period  $\Lambda_L$ :

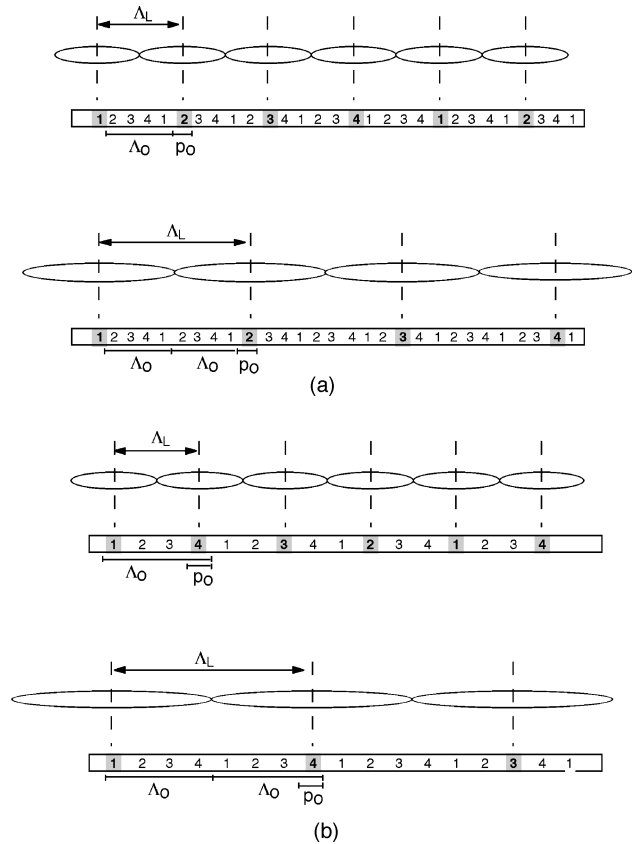


**Fig. 2** Examples for an object motif consisting of “1234.” If one lens images the 1, the next neighboring lenses (left and right) should image the 4 or 2 to generate a complete moiré image of the object motif. However, the 4 or 2 portion might be next to 1 or at a certain distance.

$$|p_i| = \Lambda_L. \tag{2}$$

The relation between the image size  $p_i$ , the object portion  $p_o$  and the position of the object array  $s_o$  is given by the image equation

$$m = \frac{p_i}{p_o} = \frac{\pm \Lambda_L}{p_o} = - \frac{f}{s_o - f}, \tag{3}$$

wherein  $f$  is the focal length.<sup>6</sup> Figure 3 illustrates the imaging properties of a single positive lens. As a consequence of Eqs. (2) and (3), the marginal rays marked as lines 1 and 2 in Figure 3 define the object size  $p_o$ . Lines 3 and 4 define the image size  $p_i$ . Depending on the object distance  $s_o$ , the image  $p_i$  is either erect ( $f > s_o > 0$ ;  $m > 1$ ) or inverted ( $s_o > f$ ;  $m < 0$ ). For an object position  $0 < s_o < 2f$ , the image  $p_i$  is magnified ( $|m| > 1$ ); for  $s_o > 2f$ , the image is demagnified ( $0 < |m| < 1$ ).

We obtain four different types of moiré image, as shown in Table 1. Depending on the object position  $s_o$ , the image part  $p_i$  might be virtual erect or real inverted. Depending on the difference in period of  $\Lambda_o$  and  $\Lambda_L$  the image sequence might be direct or reversed. Therefore, we obtain four different types of moiré images as shown in Table 1. Only in

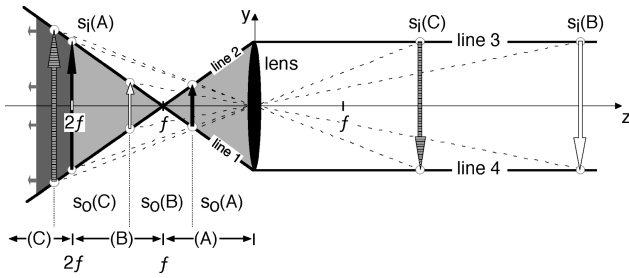


**Fig. 3** Imaging properties of a single lens of the lens array shown in Figure 1. Three different object positions are possible: (position A) the object is located at a distance  $|f| > |s_o(A)| > 0$  and generates a virtual, erect image ( $m > 1$ ) at a distance  $s_i(A)$ ; (position B) the object is located at a distance  $|2f| > |s_o(B)| > |f|$  and generates a real, inverted image ( $m < -1$ ) at a distance  $s_i(B)$ ; and (position C) the object is located at a distance  $|\infty| > |s_o(C)| > |2f|$  and generates a real, inverted image ( $-1 < m < 0$ ) at a distance  $s_i(C)$ .

cases (I) and (IV) is the appearing moiré image identical to the object motif. A graphical explanation of moiré imaging is shown in Figure 4.

**3 Erect Moiré Pattern**

For virtual erect images, the object array is located at a distance  $f > s_o > 0$ . Each lens forms a virtual erect image of the related object portion  $p_o$  as shown in Figure 4(a). If lens  $j$  images the portion  $p_k$  of the object, the next lens of order  $j + 1$  should image the portion  $p_{k+1}$  from the next participating object. The size of  $p_k$  is equal to  $p_{k+1}$ . Since the size of the image portion  $p_i$  is equal to the lens period  $\Lambda_L$  [Eq. (2)], the distance between two imaged portions is equal to  $\Lambda_L$  given by:

$$\Lambda_L = p_k + d_r + p_k + d_l + n\Lambda_O, \tag{4}$$

where,  $n\Lambda_O$  is the distance between two participating objects,  $d_l$  and  $d_r$  are nonimaged parts of the object related to lens  $j$ , and  $n$  is an integer number ( $n \geq 0$ ). Since one object period is given by  $\Lambda_O = p_k + d_r + d_l$ , the size of the object portion  $p_{erect}$  for erect moiré imaging is given by,

$$p_{erect} = \Lambda_L - N\Lambda_O, \tag{5}$$

where  $N = n + 1$  is an integer number  $\geq 1$ . For all values of  $s_o$  in the range  $f > s_o > 0$ , the size of the object portion  $p_{erect}$

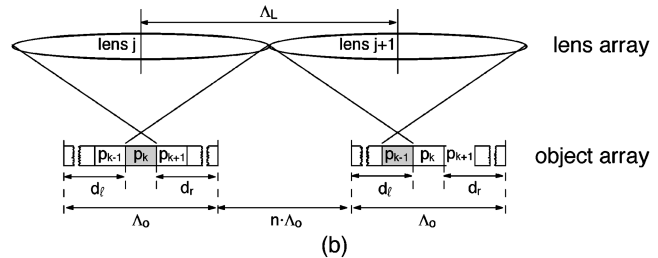
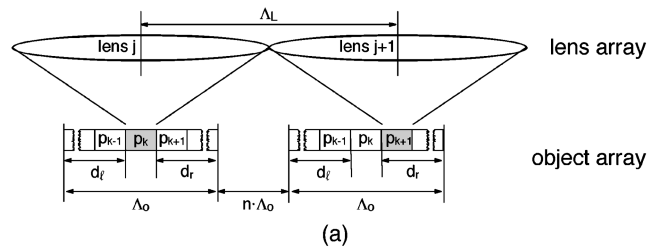


**Fig. 4** Formation of the (a) erect and (b) inverted moiré images. An object array of period  $\Lambda_O$  is partially imaged by a lens array of period  $\Lambda_L$ . Here  $n\Lambda_O$  is the distance between two arbitrary objects parts participating in building up the moiré image, and  $n$  is an integer number ( $n \geq 0$ ). Let the object be divided into equal portions of size  $p$  given by the image Eq. (3), then  $d_r$  is the distance from the right of  $p_k$  to the right end of the object element, and  $d_l$  is the distance from the left of  $p_k$  to the left end of the same object element. (a) For erect moiré imaging, the two arrays are separated by a distance  $f > s_o > 0$ . The lens  $j$  images the  $k$ th portion  $p_k$  of the first participating object. The lens of order  $j + 1$  images the portion  $p_{k+1}$  from the next participating object. (b) For inverted moiré imaging, the two arrays are separated by a distance  $\infty > s_o > f$ . The lens  $j$  images the  $k$ th portion  $p_k$  of the first participating object. The lens of order  $j + 1$  images the portion  $p_{k-1}$  of the next participating object.

is less than the period of the lens array,  $0 < p_{erect} < \Lambda_L$ , giving  $m > 1$ . Substituting in the preceding inequality from Eq. (3), the limits of the integer  $N$  for the erect magnified moiré pattern is obtained as,

$$0 < N_{erect} < \frac{\Lambda_L}{\Lambda_O}. \tag{6}$$

Erect magnified moiré images are observed only if the lens period  $\Lambda_L$  is larger than object period  $\Lambda_O$ . Each value of  $N$  corresponds to a different moiré magnification at a different object array position  $s_o$ .

**4 Inverted Moiré Pattern**

The second case to be analyzed is the condition for obtaining inverted moiré images. The problem is treated in a way similar to that for erect moiré images. For inverted images, the object array is located at a distance  $\infty > s_o > f$ . As shown in Figure 4(b), each lens images the related object portion  $p_o$ . If lens  $j$  images the portion  $p_k$  of the object array, the next lens  $j + 1$  should image the portion  $p_{k-1}$  from the next participating object. The size of the image portion  $p_i$  is equal to the lens period  $\Lambda_L$  [Eq. (2)] and given by

$$\Lambda_L = d_r + d_l + n\Lambda_O, \tag{7}$$

**Table 1** Different types of superimposed moiré images.

	Figure 2a	Figure 2b
$f > s_o > 0$ ; $p_i = +\Lambda_L$ ; erect image	<b>1 2 3 4 1 2</b> (I) moiré image = object motif	<b>4 3 2 1 4 3</b> (II) moiré image $\neq$ object motif
$s_o > f$ ; $p_i = -\Lambda_L$ ; inverted image;	<b>1 2 3 4 1 2</b> (III) moiré image $\neq$ object motif	<b>4 3 2 1 4 3</b> (IV) moiré image = object motif

Depending on the object position  $s_o$ , the image parts,  $p_i = 1, 2, 3$ , or 4 might be erect or inverted. Only in cases (I) and (IV), the moiré image is identical to the object motif.

where  $n\Lambda_O$  is the distance between two participating objects,  $d_l$  and  $d_r$  are the nonimaged parts of the object related to lens  $j$ , and  $n$  is an integer number ( $n \geq 0$ ). The integer number  $n$  gives the number of notparticipating objects in between two participating objects. Since one object period is given by  $\Lambda_O = p_k + d_r + d_l$ , the size of the object portion  $p_{\text{inverted}}$  for inverted moiré imaging is given by,

$$p_{\text{inverted}} = N\Lambda_O - \Lambda_L, \tag{8}$$

where  $N = n + 1$ , is an integer number  $\geq 1$ . The condition for inverted moiré imaging is  $\infty > s_o > f$ . As shown in Figure 3, the size of the object portion  $p_o$  is defined by line 1 and 2. Three different object positions  $s_o$  are possible.

First, for  $2f > s_o > f$ , the size of the object portion is less than the pitch of the lens array,  $0 < p_o < \Lambda_L$ , leading to  $m < -1$ . Substituting for  $p_o$  from Eq. (8), the limits of the integer  $N \geq 1$  for the inverted magnified moiré pattern is obtained as,

$$\frac{\Lambda_L}{\Lambda_O} < N < \frac{2\Lambda_L}{\Lambda_O}. \tag{9}$$

From Eqs. (8) and (9), we find that inverted moiré magnification could be observed according to the following conditions:

1. The lens period  $\Lambda_L$  is larger than the object period  $\Lambda_O$ . For the same values of  $\Lambda_L$  and  $\Lambda_O$  inverted moiré magnification can be observed for different object positions depending on the value of  $N$ .
2. The lens period  $\Lambda_L$  is smaller than the object period  $\Lambda_O$ . Inverted moiré magnification is only observed for  $N = 1$  and  $\Lambda_L < \Lambda_O < 2\Lambda_L$ .

Second, for  $s_o = 2f$  (antiprincipal planes position), the size of the object portion  $p_o$  is equal to the period of the lens array  $\Lambda_L$ , leading to  $m = -1$ . The composite image consists of locally inverted parts of the object. If the object period  $\Lambda_O$  is equal to the lens period  $\Lambda_L$ , a pattern similar to case III in Table 1 is observed.

Finally, for  $\infty > s_o > 2f$ , the size of the object portion  $p_o$  is larger than the pitch of the lens array  $\Lambda_L$  and  $-1 < m < 0$ . The lower limit for of the integer  $N \geq 1$  for an inverted demagnified moiré pattern is,

$$N > \frac{2\Lambda_L}{\Lambda_O}. \tag{10}$$

### 5 Magnification

From the image Eq. (2) and Figure 3, the sign of the image portion  $p_i$  is positive or negative, corresponding to erect ( $f > s_o > 0$ ) or inverted ( $\infty > s_o > f$ ) imaging. From Eqs. (5) and (8) and the image of Eq. (3), the magnification  $m$  of a moiré magnifier is always given by

$$m = \frac{\Lambda_L}{\Lambda_L - N\Lambda_O}. \tag{11}$$

For erect imaging, the moiré image is always magnified ( $m > 1$ ). For inverted imaging, the moiré image is either magnified ( $m < -1$ ) or demagnified ( $-1 < m < 0$ ).

### 6 Image Formation and Observation

In the simplest case, a lens array of  $L \times L$  lenses and  $\Lambda_L$  lens period generates one complete magnified image of the object pattern [see Figure 1(d)]. In this case, the array size  $L\Lambda_L$  is equal to the size of the moiré image. The object pattern has been magnified by factor  $m$  and we get the condition  $L\Lambda_L = |m|\Lambda_O$ . In a more general case, the lens array generates  $I \times I$  magnified images of the object pattern, leading to

$$I = \frac{L\Lambda_L}{|m|\Lambda_O}. \tag{12}$$

From Eqs. (11) and (12) the object period  $\Lambda_O$  is given by

$$\Lambda_O = \frac{L}{NL \pm I} \Lambda_L. \tag{13}$$

The positive sign holds for virtual erect images, the negative sign holds for inverted images. For  $|\Lambda_L - N\Lambda_O| < \Lambda_L$ , a magnified image is obtained. For  $N\Lambda_O - \Lambda_L > \Lambda_L$ , a demagnified image is obtained. Each value of  $\Lambda_O$  corresponds to a different object array position  $s_o$  given by

$$s_o = fN \frac{\Lambda_O}{\Lambda_L}. \tag{14}$$

The size of the magnified image  $m\Lambda_O$  is given by

$$m\Lambda_O = \frac{\Lambda_O}{\pm(\Lambda_L - N\Lambda_O)} \Lambda_L. \tag{15}$$

The number of object patterns  $O$ , in one dimension, that contribute to one moiré image is equal to the magnification  $m$ ,

$$O = |m|. \tag{16}$$

The number of lenses  $L/I$ , in one dimension, that generate one moiré image is given by

$$\left| \frac{L}{I} \right| = \left| \frac{\Lambda_O}{p_o} \right| = \left| \frac{\Lambda_O}{\Lambda_L - N\Lambda_O} \right|. \tag{17}$$

The moiré image generated by a moiré magnifier could be observed on a screen located at the image distance  $s_i$ , given by

$$s_i = - \frac{Nf\Lambda_O}{\Lambda_L - N\Lambda_O}. \tag{18}$$

As a consequence of Eq. (2), the moiré image can be observed by the naked eye at any position behind the lens.

For virtual erect moiré images, if the observer moves transversely to the lens array, the image appears to move in

**Table 2** Numerical example for a lens array period  $\Lambda_L = 9 u$  and object array period  $\Lambda_O = 4 u$  (arbitrary length-unit  $u$ ): the possible values of  $N$  satisfying the moiré magnifier inequalities for  $\Lambda_L / \Lambda_O = 9/4$ .

Type of Moiré Image	Virtual Erect Magnified	Real Inverted Magnified	Real Inverted Demagnified
Condition	$0 > N > \frac{9}{4}$	$\frac{9}{4} > N > \frac{18}{4}$	$\frac{18}{4} < N$
$s_o$	$0 > s_o > -f$	$-f > s_o > 2f$	$-2f > s_o$
Value of $N$	$a$ $b$	$a$ $b$	$5$
Object array position $s_o$	$-\frac{4}{9} f$	$-\frac{8}{9} f$	$-\frac{20}{9} f$
Object array portion $p_o$	$5u$	$1u$	$11u$
Magnification $m$	$\frac{9}{5}$	$9$	$-\frac{9}{11}$

the same direction. For inverted moiré pattern, the image moves in the opposite direction. This corresponds to the sign of the magnification factor  $m$  as indicated in Eq. (15).

A numerical example describing the generation of three different types of moiré images can be obtained by considering a moiré magnifier system consisting of a lens array period  $\Lambda_L = 9 u$  and object array of period  $\Lambda_O = 4 u$ , where  $u$  is an arbitrary length unit. Table 2 shows numerically the possible values of  $N$  satisfying the moiré magnifier inequalities [Eqs. (6), (9), and (10)], for  $\Lambda_L / \Lambda_O = 9/4$ . For each value of  $N$ , the object position  $s_o$  and its corresponding object portion  $p_o$  and magnification  $m$  are calculated. Considering that the object array motif of the above moiré magnifier system consists of 1234, the Figures 5, 6 and 7

describe the generation of the different magnified images corresponding to different object array positions  $s_o$ . Figure 5 shows the possible erect magnified moiré images, which are corresponding to the object array position  $0 < |s_o| < f$ . Figure 5(a) corresponds to  $N=1$  and Figure 5(b) to  $N=2$ , as given in Table 2. Figure 6 shows the possible inverted magnified moiré images which are corresponding to the object array position  $f < |s_o| < 2f$ . Figure 6(a) corresponds to  $N=3$  and Figure 6(b) to  $N=4$ . Figure 7 shows an inverted demagnified moiré image which corresponds with the object array position,  $2f < |s_o|$  and  $N=5$ .

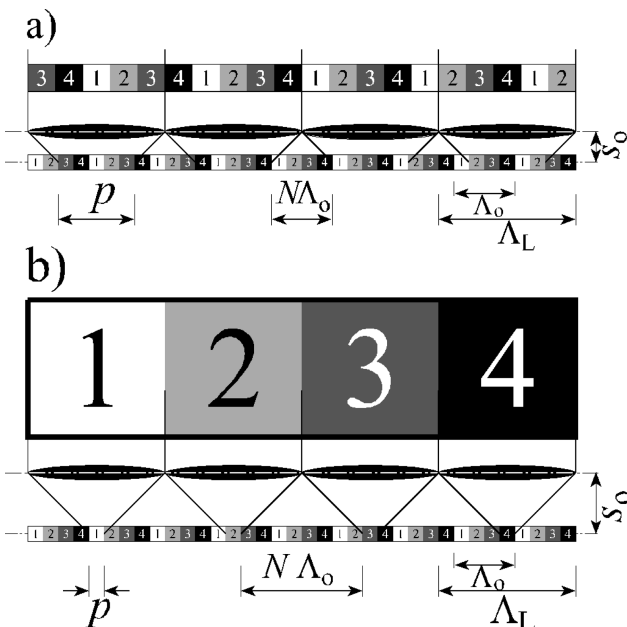


**Fig. 5** Erect magnified moiré images corresponding to the object array position  $0 < |s_o| < f$  and (a) the values  $N=1$  and (b)  $N=2$ , as shown in Table 2.

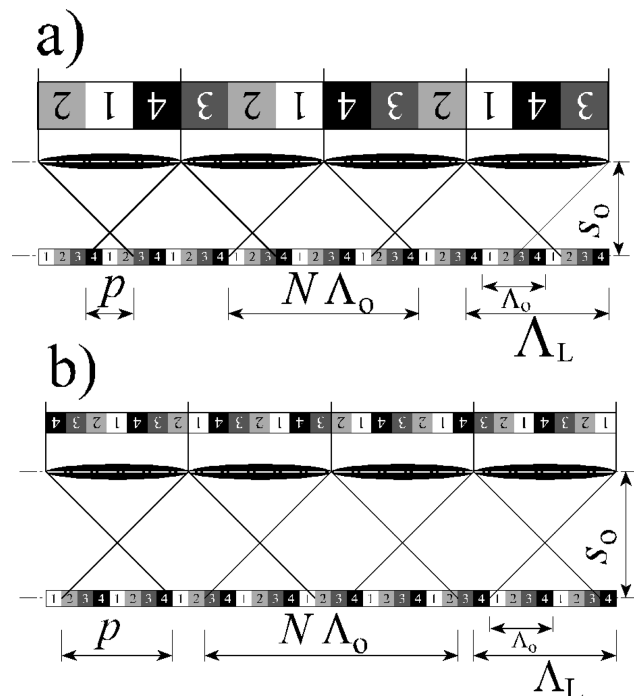


**Fig. 6** Inverted magnified moiré images corresponding to the object array position  $f < |s_o| < 2f$  and (a) the values  $N=3$  and (b)  $N=4$ , as shown in Table 2.

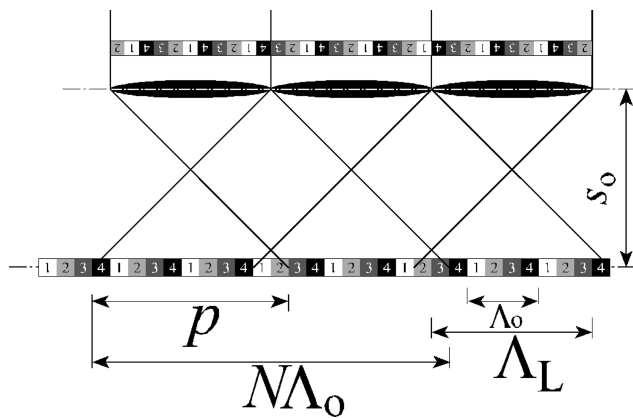


**Fig. 7** Inverted demagnified moiré image corresponding to the object array position  $2f < |s_o|$  and the value  $N=5$ , as shown in Table 2.

The mathematical relations derived in this paper were confirmed experimentally. We used a square lattice lens array of converging lenses. The size of the lens array is  $42.73 \times 42.73$  mm, its period  $\Lambda_L$  is 1.07 mm, and the focal length  $f$  is 2.43 mm. Object arrays with different periods  $\Lambda_O$  are computer generated and printed onto a transparency using a laser printer. The scheme of the experimental setup is shown in Figure 8. Diffused white light is used to illuminate the moiré magnifier system. The object array is placed in front of the lens array. The lens array is attached to a microtranslation stage to move it longitudinally in the  $z$ -direction and to adjust the object array distance  $s_o$ . The real moiré images are projected on a screen and then recorded by a camera connected to a computer. In case of virtual moiré images, the images are received directly by the camera. Table 3 shows the different object array periods  $\Lambda_O$  with their corresponding selected value of  $N$  and positions  $s_o$ . The resulting magnification and image type are also given for an aligned position. The experimental values are obtained from the recorded images. A selection of the resultant images is shown in Figures 9, 10, and 11. The object pattern is shown on left and the observed moiré pattern on the right.

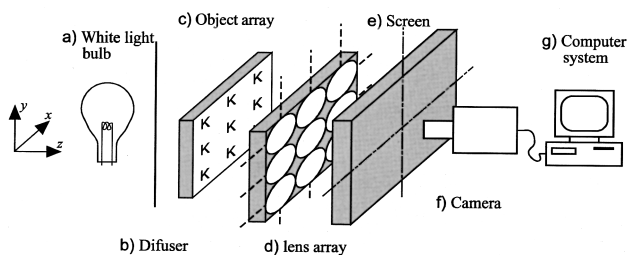


**Fig. 8** Experimental setup used for testing moiré magnifiers. The object array is placed in front of the lens array and illuminated by diffused white light. The lens array is moved longitudinally in the  $z$ -direction and to adjust the object-to-lens distance  $s_o$ . The real moiré images are projected on a screen and then recorded by a camera connected to a computer. In the case of virtual moiré images, the images are received directly by the camera.

**Table 3** Theoretical and experimental values of the magnification for three object array motifs consisting of L, A and K used to generate three different types of moiré images, where the period of the lens array is  $\Lambda_L = 1.07$  mm and its focal length is  $f = 2.43$  mm.

Object Pattern	L	A	K
Array period, $\Lambda_O$ (mm)	1.32	4.00	0.97
Value of $N$	1	1	1
Object position $ s_o $ (mm)	3.00	9.08	2.20
Type of moiré image	Real inverted magnified	Real inverted demagnified	Virtual erect magnified
Theoretical magnification	-5.00	-0.40	8.40
Experimental magnification	-4.81	-0.38	8.46

### 7 Translation and Rotation

In the preceding analysis an aligned moiré magnifier is considered; that is, the axes of both object and lens array are parallel and coincident. If the lens is translated with respect to the object array, the moiré pattern appears to move. Each lens images another part of the related object. The direction of the movement depends on the relative motion of the arrays, the lens period  $\Lambda_L$ , the object period  $\Lambda_O$ , and the value of  $N$  and is described by Eq. (15). From the experiment we can observe that for real moiré images, the resultant translation and rotation are in the same direction as those of the object array, although it is in the opposite direction for virtual patterns, as we could expect from the sign of the magnification. The apparent motion speed of the resulting moiré image is proportional to the magnification value.

Moiré magnification is based on a periodically repeated object pattern imaged by a periodically repeated array of identical lenses. The object period is the shortest distance between two identical parts of adjacent object unit cells along the lens array axes. Assume that we have an aligned configuration where moiré magnification appears. If the lens array (or the object array) is rotated by a small angle, then the moiré image rotates and changes its magnification. For larger rotations, the moiré image might disappear and reappear at certain angles.

If one of the two arrays is rotated an angle  $\Theta$  relative to the other, the distance to the next identical object part located on the lens axis will change. Accordingly, a new rectangular lattice of the object array, aligned with the lens array grid, with a new period is created at a certain rotation

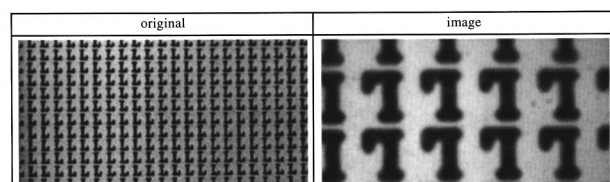


**Fig. 9** Object and image plane for a situation of real inverted magnified moiré patterns as described in Table 3.

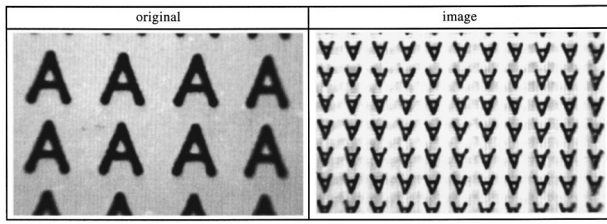


**Fig. 10** Object and image plane for a situation of real inverted demagnified moiré patterns as described in Table 3.

angle. The new period ratio  $\Lambda_L/\Lambda_{O,new}$  may or may not satisfy the moiré magnifier requirements at the same object array position  $s_o$ . Therefore, moiré magnified images may appear and disappear as the object rotates.

Let assume a square grid of object with period  $\Lambda_o$  that produces a moiré magnifier effect for a given position. A new square grid of repeated objects is obtained when the object rotates and the rotation angle obeys the following relation (see Figure 12),

$$\Theta = \tan^{-1}\left(\frac{y}{x}\right), \tag{19}$$

where  $x$  and  $y$  are integer numbers greater than or equal to 0 ( $\Theta$  changes from 0 to  $90^\circ$ ). The new object array, aligned with the lens array, has a new pitch, which is equal to

$$\Lambda_{O,new} = \Lambda_o \frac{x}{\cos \Theta} = \Lambda_o \frac{y}{\sin \Theta} = \Lambda_o(x^2 + y^2)^{1/2}. \tag{20}$$

Thus, the varying rotation angles create new periods ratios, which define different moiré pattern characteristics.

An aligned position in which moiré magnification appears has a fixed value of  $N$ . If the distance between the two arrays remains unchanged then the imaged portion  $p$  will be the same although one of the two arrays rotates with respect to the other,

$$|p| = |\Lambda_L - N\Lambda_o| = |\Lambda_L - N_{new}\Lambda_{O,new}|. \tag{21}$$

From this equation and Eq. (20) the condition to obtain moiré magnification after rotation becomes

$$N_{new} = \frac{N}{(x^2 + y^2)^{1/2}}, \tag{22}$$

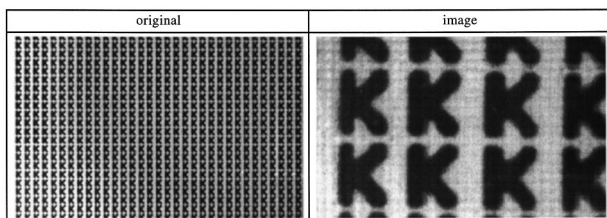


**Fig. 11** Object and image plane for a situation of virtual erect magnified moiré patterns as described in Table 3.

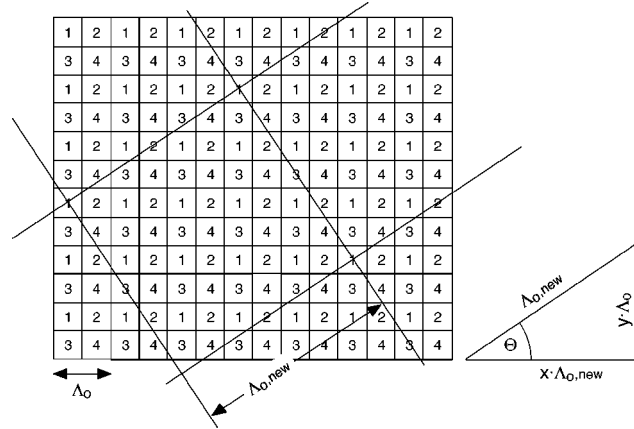


**Fig. 12** Rotation of the object array. A symmetric square array of identical objects (1234) produces a new object period  $\Lambda_{O,new}$  for a rotation by an angle  $\Theta$ .

which is a very restricted condition to be fulfilled by the involved integer numbers. It is clear from Eq. (11) that the magnification depends on the imaged portion and the lens pitch. So the magnification will remain constant for different rotation angles at the same object array position  $s_o$ .

### 8 Summary

If an array of identical lenses is used to view an array of identical objects, the phenomena of moiré magnification might occur. For certain array positions, a magnified image of the repeated object pattern is observed on a screen or by eye. The moiré image might be erect or inverted, magnified or demagnified. A shift in  $z$  or a rotation in  $\theta$  of the lens array versus the object array might generate a different magnified pattern. The object position in  $z$  and  $\theta$ , which is necessary to observe a magnified moiré image, is related to the difference in the array periods. A demagnified moiré image is observed when the object period exceeds the lens period and the object array is located at a distance exceeding twice the focal length.

As one moves across the lens array, the moiré image appears to move in the same direction in case of virtual erect moiré pattern and in the opposite direction in case of real inverted moiré pattern.

The mathematical relations are in good agreement with the experiments performed for all three types of moiré magnified patterns.

### Acknowledgement

One of the authors (Hala Kamal) is grateful to the Institute of Microtechnology (IMT), Université de Neuchâtel, and the Universidad Complutense de Madrid for their support of her visit at IMT.

### References

1. M. E. Knotts, R. G. Hemphill, M. E. Knotts, "moiré or Moiré?" *Opt. Photon. News* **7**(8), 53–55 (Aug. 1996).
2. O. Kafri and L. Glatt, *The Physics of Moiré Metrology*, John Wiley and Sons, New York (1990).
3. G. Indebetouw and R. Czarnek, Eds. Selected Papers on Optical Moiré and Applications, SPIE Milestone Series, Vol. MS 64, SPIE, Bellingham, WA (1992).
4. M. C. Hutley, R. F. Stevens and P. Savander, "The moiré magnifier," *Pure Appl. Opt.* **3**, 133–142 (1994).
5. O. Mikami, *Jpn. J. Appl. Phys.* **14**, 417–418, 1065–1066 (1975).

6. N. Davies and M. McCormick, "The use of microlens arrays in integral photography," in *Proc. IOP Short Meetings No. 30*, pp. 109–122, Teddington, UK (1991).
7. N. Davies and M. McCormick, "Three dimensional optical transmission and micro optical elements," in *Miniature and Micro-Optics and Micromechanics, Proc. SPIE 1992*, 247–257 (1993).
8. K. Hamanaka, H. Koshi, and M. Toyama, "An artificial compound eye using a two-dimensional array of Selfoc lenses and its application to a scale-invariant image sensor," in *Tech. Digest of MOC'95*, pp. 94–97, Optical Society of Japan, Hiroshima (1995).
9. J. S. Sanders, *Selected Papers on Natural and Artificial Compound Eye Sensors*, SPIE Milestone Series, Vol. 122, SPIE, Bellingham, WA (1996).
10. W. Shaomin and L. Ronchi, *Principles and Design of Optical Arrays*, Progress in Optics XXV, pp. 279–348, Amsterdam, Netherlands (1988).



**Hala Kamal** graduated in physics in 1989 from the Faculty of Science, Ain Shams University, Cairo, Egypt, where she has been working since graduation. In 1994 she obtained a scholarship from the Spanish Ministry of Education and Science to get her PhD. Currently she is finishing her PhD under the supervision of Dr. Alda in the field of the design of optical arrays at the Universidad Complutense de Madrid.

During the periods from September to December 1996 and from July to September 1997 she was a visiting research fellow at the Institute of Microtechnology, Neuchâtel, Switzerland, where she worked in the field of moiré magnifiers.



**Reinhard Völkel** received his diploma in physics in 1989 and his PhD in 1994, both from the University of Erlangen-Nürnberg, Germany, where he worked on holographic optical elements and optical interconnects for high-speed telecommunication systems. He joined the Institute of Microtechnology at the Université de Neuchâtel, Switzerland, in 1994. His current research activities are fabrication and testing of micro-optics, miniaturized imaging

systems, novel photolithographic techniques such as microlens projection lithography and smart mask lithography, bio-inspired eye sensors, micro-optics for microTAS and chemical microchips, and assembling, alignment and bonding techniques for optical microsystems.



**Javier Alda** received the LicSc degree in 1985 from the University of Zaragoza and the PhD degree in physics in 1988 from the Universidad Complutense de Madrid. He is currently a professor of optics at the School of Optics, where he has been teaching since 1985. His principal interests are laser beam propagation and industrial inspection systems.